Validation of an approximate model for the thermal behavior in acoustically driven bubbles

Laura Stricker[a)]
Physics of Fluids Group, Faculty of Science and Technology, Impact and Mesa+ Institutes and Burgers Center for Fluid Dynamics, University of Twente, 7500AE Enschede, The Netherlands

Andrea Prosperetti[b)]
Department of Mechanical Engineering, Johns-Hopkins University, North Charles Street, Baltimore, Maryland 21218

Detlef Lohse
Physics of Fluids Group, Faculty of Science and Technology, Impact and Mesa+ Institutes and Burgers Center for Fluid Dynamics, University of Twente, 7500AE Enschede, The Netherlands

(Received 16 December 2010; revised 9 March 2011; accepted 9 March 2011)

The chemical production of radicals inside acoustically driven bubbles is determined by the local temperature inside the bubbles. Therefore, modeling of chemical reaction rates in bubbles requires an accurate evaluation of the temperature field and the heat exchange with the liquid. The aim of the present work is to compare a detailed partial differential equation model in which the temperature field is spatially resolved with an ordinary differential equation model in which the bubble contents are assumed to have a uniform average temperature and the heat exchanges are modeled by means of a boundary layer approximation. The two models show good agreement in the range of pressure amplitudes in which the bubble is spherically stable. © *2011 Acoustical Society of America*. [DOI: 10.1121/1.3626132]

PACS number(s): 43.35.Vz, 43.35.Ei, 43.25.Yw [CCC] Pages: 3243–3251

I. INTRODUCTION

In acoustically driven microbubbles extreme conditions of temperature and pressure can emerge, giving rise to chemical reactions, involving the gas inside the bubbles and the surrounding liquid ("sonochemistry," see, e.g., Refs. 1–6). Even without bubble-bubble interaction—i.e., in the case of a single isolated acoustically trapped bubble as in single-bubble sonoluminescence[7–11]—the fluid- and thermodynamics is still rather complex. Even if such a bubble remains spherical (i.e., is small enough and weakly enough driven), a complete description of the process still must take into account spatial pressure and temperature distribution both inside and outside the bubble, mass, and heat diffusion, evaporation/condensation phenomena, change in transport parameters due to thermal and compositional changes of the mixture, inertial effects, as well as all chemical reactions of the unstable species in the bubble. Various models with an increasing degree of sophistication exist, see, e.g., Refs. 12–20 and for a review, Ref. 11. Clearly, the complexity of the process implies the need of simplifications when addressing practical problems, such as studying the chemical output.

In this paper we focus on the thermal behavior (achieved temperatures, heat fluxes in and out of the bubble), which governs the chemical reactions by Arrhenius' law. We want to compare the results from the numerical solutions of the advection-diffusion partial differential equation (PDE) for the temperature field inside the bubble as described by Prosperetti and co-workers[12,21] and others[22–24] with the results from a thermal boundary layer approximation of the full dynamics, which leads to the ODE model which has been developed in Twente.[19,20,25] As such ordinary differential equation (ODE) models are computationally much cheaper than solving the full PDEs of the gas flow inside the bubble, they are highly desirable in order to get a quick overview on the thermal conditions inside the bubble and the resulting chemical reactions. However, such simplifying ODE models must be verified against the results from the solution of the full PDEs. Such a verification is the aim of the present paper. From a sonochemical point of view, there is a temperature range where the radical production is optimal, regardless of the ambient pressure.[26] Therefore a precise determination of applicable limits of ODE-type approximations plays a crucial role in correct quantitative estimates of production/destruction of radicals.

ODE type approximations of the gas dynamics inside acoustically driven bubbles have a tradition, see Refs. 11, 27–29. A first attempt was the adoption of the adiabatic approximation for the gas transformation with artificial increase of the liquid viscosity,[30] in order to keep into account the energy loss and the subsequent thermal damping. However, this solution was found unsatisfactory, as it overestimated the damping of nonlinear oscillations, especially the first nonlinear resonant peak. A second attempt was to consider a gas transformation with a variable isoentropic index $\kappa(t)$, depending on the instantaneous Peclet number $\mathrm{Pe}(t) = |\dot{R}(t)|R_0^2/R(t)D_g(t)$,[12,31,32] but also this model had strong limitations,[33] as it was based on linear

[a)]Author to whom correspondence should be addressed. Electronic mail: l.stricker@utwente.nl
[b)]Also at: Physics of Fluids Group, University of Twente, Enschede, The Netherlands.

oscillation approximation and it could not include the effects of subharmonic components in the response. Nonetheless, it has successfully been used in the context of single bubble sonoluminescence,[13,14,18,24,34,35] often even only with an effective polytropic exponent.

In the present work we use the ODE model based on the thermal boundary layer approximation of Refs. 19, 20, 25. It will be described in detail in Sec. II. Roughly speaking, this ODE model includes the Rayleigh–Plesset equation for the radial dynamics of the bubble, van der Waals law for the inner pressure, and the energy equation for the temperature, where the heat flux is estimated from a boundary layer approximation.

The PDE model, also described in detail in Sec. II, includes the Rayleigh–Plesset equation, an ODE equation derived from momentum and continuity equations for the evolution of the inner pressure,[32] and a PDE for the temperature, both inside and outside the bubble.

In both models we assumed a perfect gas inside the bubble, low Mach number regimes, spherical symmetry, and thus shape stability. However, while the first two assumptions are generally realistic, the last two are strictly dependent on the specific parameter regime that are considered, as large and strongly driven gas bubbles become shape unstable. This shape instability is meanwhile well understood, even quantitatively.[11,36–45] Obviously, strictly speaking our results cannot be applied to shape unstable bubbles, as such bubbles decay to smaller ones, and for those cases special care has to be paid when comparing numerical results with experimental data.

II. SUMMARY OF THE MODELS

Both models studied in this work make use of the Rayleigh-Plesset equation to describe the radial dynamics of the bubble:

$$\left(1-\frac{\dot{R}}{c_L}\right)R\ddot{R}+\frac{3}{2}\left(1-\frac{\dot{R}}{3c_L}\right)\dot{R}^2=\frac{1}{\rho_L}\left(1+\frac{\dot{R}}{c_L}+\frac{R}{c_L}\frac{d}{dt}\right)[p_B-p_A]. \tag{1}$$

Here time derivatives are denoted by a dot, R is the bubble radius, c_L and ρ_L are the speed of sound and the density of the liquid, p_B is the liquid pressure just outside the bubble surface, and p_A the ambient pressure in the liquid assumed to be given by

$$p_A = p_\infty - P_a \cos \omega t, \tag{2}$$

in which p_∞ is the static pressure and P_a the acoustic driving pressure. The period of the driving sound field is given by $\tau_d = 2\pi/\omega$. An explicit expression for p_B results from normal stress balance at the bubble wall

$$p = p_B + 4\mu_L\frac{\dot{R}}{R}+\frac{2\sigma}{R}, \tag{3}$$

with μ_L the dynamic viscosity of the liquid and σ the surface tension coefficient. The gas pressure in the bubble, p, may be regarded as spatially uniform as long as the Mach number of the bubble wall motion is not too large. In the left-hand side of Eq. (3) we have neglected the very small contributions due to the gas viscosity and the vapor pressure. As will be shown below, the temperature of the liquid at the bubble surface remains sufficiently low for this to be an excellent approximation.

The two models differ significantly in the way in which the pressure and temperature of the bubble contents are calculated. Here we provide a summary of the two formulations referring the reader to several papers for additional details and derivations.[20,44,46,47]

A. PDE model for $T(t)$

In the detailed model of Refs. 44, 46 the gas pressure is found by solving

$$\dot{p} = \frac{3}{R}\left((\gamma-1)\lambda\frac{\partial T}{\partial r}\bigg|_R - \gamma p\dot{R}\right), \tag{4}$$

where T is the gas temperature, γ is the ratio of the gas specific heats, $\lambda = \lambda(T)$ is the gas thermal conductivity, and r the radial coordinate measured from the bubble center. The temperature distribution inside the bubble is given by

$$\frac{\gamma}{\gamma-1}\frac{p}{T}\left[\frac{\partial T}{\partial t}+\frac{1}{\gamma p}\left((\gamma-1)\lambda\frac{\partial T}{\partial r}-\frac{1}{3}r\dot{p}\right)\frac{\partial T}{\partial r}\right]-\dot{p}=\nabla\cdot(\lambda\nabla T). \tag{5}$$

The derivation of this equation (see, e.g., Ref. 46) treats the gas as perfect and its pressure as spatially uniform.

The temperature in the liquid $T_L(r,t)$ is described by the standard constant-properties convection-diffusion equation neglecting compressibility effects and viscous dissipation:

$$\rho_L c_{p,L}\left(\frac{\partial T_L}{\partial t}+\frac{R^2\dot{R}}{r^2}\frac{\partial T_L}{\partial r}\right)=\lambda_L\nabla^2 T_L. \tag{6}$$

Here $c_{p,L}$ and λ_L are the liquid specific heat and thermal conductivity.

At the bubble surface continuity of temperatures and heat fluxes are assumed:

$$T(R(t),t) = T_L(R(t),t), \tag{7}$$

$$\lambda\frac{\partial T}{\partial r}(R(t),t) = \lambda_L\frac{\partial T_L}{\partial r}(R(t),t). \tag{8}$$

The gas temperature is assumed to be regular at the bubble center $r = 0$ and the liquid temperature to remain undisturbed at the initial value T_∞ far from the bubble.

B. ODE model for $T(t)$

This model[19,20] makes no attempt to describe the spatial distribution of the gas temperature inside the bubble. Rather, it is formulated in terms of a volume-averaged value $\langle T\rangle$ determined by a global balance over the bubble volume expressing the first principle of thermodynamics:

$$c_v m_g \langle \dot{T} \rangle = Q - p\dot{V}, \tag{9}$$

where m_g is the mass of gas inside the bubble, c_v is the constant-volume specific heat of the gas, and $V = \frac{4}{3}\pi R^3$ is the bubble volume. The net heat absorbed by the bubble per unit time is modeled as

$$Q = 4\pi R^2 \lambda \frac{T_\infty - \langle T \rangle}{l_{\text{th}}} \tag{10}$$

with l_{th} an estimate of the thickness of the thermal boundary layer in the liquid. A correct prescription for this quantity is crucial for the physical realism of the model. The general properties of diffusion processes suggest

$$l_{\text{th}} = \sqrt{D\tau_{\text{th}}} \tag{11}$$

in which D is the gas thermal diffusivity evaluated for $T = T_\infty$ and τ_{th} an appropriate time scale which is chosen as $\tau_{\text{th}} = R/|\dot{R}|$. A cutoff is required when $\dot{R}$ becomes too small. A consideration of the Fourier series solution of the diffusion equation in a bubble of constant radius (which is appropriate when $\dot{R}$ is small) leads to the estimate $l_{\text{th}} = R/\pi$. In conclusion, the final expression for the estimate of the boundary layer is[19,20]

$$l_{\text{th}} = \min\left(\sqrt{\frac{RD}{|\dot{R}|}}, \frac{R}{\pi}\right). \tag{12}$$

The gas pressure is obtained from a form of the van der Waals equation of state modified to take into account inertial effects of the gas:

$$p = \frac{N_{\text{tot}} k_B \langle T \rangle}{V - N_{\text{tot}} B} - \frac{1}{2}\langle \rho \rangle R\ddot{R}, \tag{13}$$

where $\langle \rho \rangle$ is the volume-averaged gas density, N_{tot} the total number of gas molecules, k_B the Boltzmann constant, and B the molecular covolume.

III. NUMERICAL METHOD

The gas energy equation (5) of the detailed model is first reduced to a more manageable form by introducing the auxiliary variable

$$\tilde{T} := \frac{1}{\lambda(T_\infty)} \int_{T_\infty}^{T} \lambda(T')dT'. \tag{14}$$

After this step, the numerical solution of the model is carried out by first transforming it into a set of ordinary differential equations by a collocation procedure as described in Ref. 12 and, in greater detail, in Ref. 21. We set

$$\frac{\tilde{T}}{T_\infty} \approx \sum_{k=0}^{N} a_k(t) T_{2k}(y), \tag{15}$$

where $y = r/R(t)$ and the T_{2k} are even Chebyshev polynomials. The variable y fixes the boundary at $y = 1$ and the use of even polynomials guarantees a vanishing gradient at the bubble center $y = 0$. The expansion (15) is substituted into the gas energy equation written in terms of $\tilde{T}$ and the result evaluated at the Gauss–Lobatto collocation points y_k

$$y_k = \cos(\pi k/2N), \quad k = 0, 1, ..., N. \tag{16}$$

Before subjecting the liquid energy equation to a similar treatment, the semi-infinite range $R(t) \le r < \infty$ is mapped onto the finite range $1 \ge \xi \ge 0$ by the coordinate transformation

$$\frac{1}{\xi} = 1 + \frac{r/R(t) - 1}{l}. \tag{17}$$

The length l is a measure of the thermal diffusion length in the liquid and is taken as

$$l = \ell \frac{\sqrt{D_L/\omega}}{R_0}, \tag{18}$$

with D_L the liquid thermal diffusivity $D_L = \lambda_L/c_{p,L}\rho_L$ and ℓ a numerical constant. On the basis of the results described in Ref. 21 a value of $\ell = 20$ has been used in this work. After recasting the liquid energy equation (6) in terms of the new variable ξ, the liquid temperature is expanded in a truncated Chebyshev series similar to Eq. (15):

$$\frac{T_L}{T_\infty} \approx \sum_{k=0}^{M} b_k(t) T_{2k}(\xi), \tag{19}$$

substituted into the equation and the result evaluated at the Gauss–Lobatto collocation points ξ_j

$$\xi_j = \cos(\pi j/2M), \quad j = 0, 1, ..., M. \tag{20}$$

Use of the even polynomials in Eq. (19) enforces the temperature condition at infinity in the form $\partial T_L/\partial r \to 0$ as $\xi \to 0$, i.e., as $r \to \infty$

The interface conditions (7) and (8), as written, are algebraic constraints among the unknown coefficients of the expansions (15) and (19). For numerical purposes it proves convenient to differentiate them with respect to time to find

$$\frac{\lambda(T_\infty)}{\lambda(T_s)} \sum_{k=0}^{N} \dot{a}_k = \sum_{j=0}^{M} \dot{b}_j, \tag{21}$$

$$\sum_{\ell=0}^{N} 4\ell^2 \dot{a}_\ell = -\frac{1}{l}\frac{\lambda_L}{\lambda(T_\infty)} \sum_{n=1}^{M} 4n^2 \dot{b}_n, \tag{22}$$

where T_s is the bubble surface temperature.

These steps reduce the detailed model to a system of ordinary differential equations, the N equations for a_k arising from the collocation of the gas energy equation, the M equations for b_k arising from the collocation of the liquid energy equation, the two boundary conditions (21) and (22), the Rayleigh–Plesset radial equation (1) and the pressure equation (4). These equations (and notably those including the

time derivatives of the temperature expansion coefficients) constitute a coupled linear system which is first solved for the derivatives by Gaussian elimination and then integrated in time by using the 6th order Gear stiff solver implemented in the IMSL libraries.[48]

In order to ascertain the accuracy of the time integration we monitored the ratios of the coefficients of the last to the first terms in the expansions $|a_N/a_1|$ and $|b_M/b_1|$, checking that they remained smaller than 10^{-6} and 10^{-4}, respectively, at all times. We found that 20 and 30 terms, respectively, for the gas and liquid temperature fields were sufficient to meet these condition.

To simplify the inverse mapping between the modified and original gas temperatures $\tilde{T}$ and T the temperature dependence of the gas thermal conductivity was approximated by a linear relation

$$\lambda = A + CT. \tag{23}$$

The values $A = 0.01165$ W/mK and $C = 5.528 \times 10^{-5}$ W/mK^2 approximate the measured thermal conductivity of air over the range 200 K $\leq T \leq$ 3000 K.[12]

The other numerical values used in the simulations described in the next section were $c_L = 1481$ m/s, $\rho_L = 1000$ kg/m^3, $\mu_L = 10^{-3}$ kg/ms, $\sigma = 0.072$ N/m, $c_{p,L} = 4182$ J/kg K, $\lambda_L = 0.59$ W/mK, and $B = 5.1 \times 10^{-29}$ m^3. These values are appropriate for an air-water system at normal temperature and pressure, $T_\infty = 293.15$ K and $p_\infty = 101.3$ kPa.

IV. RESULTS

The results that follow refer to a sound frequency of 20 kHz, which is typical of much sonochemical work.[49] According to the theoretical results of Refs. 29, 39, 41, 44 which were later experimentally confirmed,[43,45] at this frequency a 50 and a 100 μm-radius bubble become spherically unstable at pressure amplitudes on the order of 30 and 15 kPa, respectively. At pressure amplitudes slightly above this threshold the bubble will develop shape oscillations superimposed on the volume mode. These oscillations lead to a breakup of the bubble at still higher amplitudes which it is difficult to quantify as they depend on various factors such as the perturbations induced by other bubbles, liquid motion and others. Even in the regime of weak shape oscillations a spherically symmetric model will capture the major effect responsible for the heating of the gas, namely, the compression of the bubble. For this reason, and in order to bring out more clearly the differences between the two models, we will use pressure amplitudes of both 20 and 70 kPa.

The latter case $P_a = 70$ kPa is shown in Fig. 1 for $R_0 = 130$ μm and $f = 20$ kHz. These conditions are close to resonance as for a $R_0 = 130$ μm bubble the linear natural frequency is approximately 24.4 kHz. The bubble executes strong volume pulsations with a maximum radius of about 3 times R_0, which corresponds to a maximum volume more than two orders of magnitude larger than the equilibrium volume. In contrast, for $P_a = 20$ kHz only very gentle oscillations are observed (not shown). In both cases the differences between the ODE model and the PDE model are very small as can be seen in Fig. 1 for the $P_a = 70$ kPa case (for the $P_a = 20$ kPa case the differences are hardly detectable).

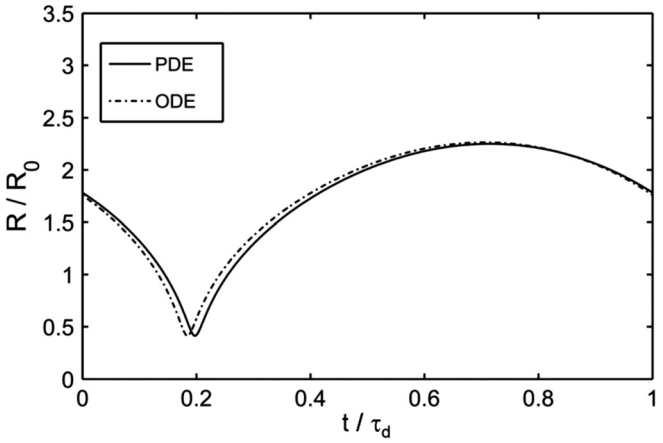

FIG. 1. Comparison between the temporal evolution of the normalized radius during the steady oscillations of an air bubble with an equilibrium radius of 130 μm driven at 70 kPa and 20 kHz as predicted by the detailed (solid line) and simplified models.

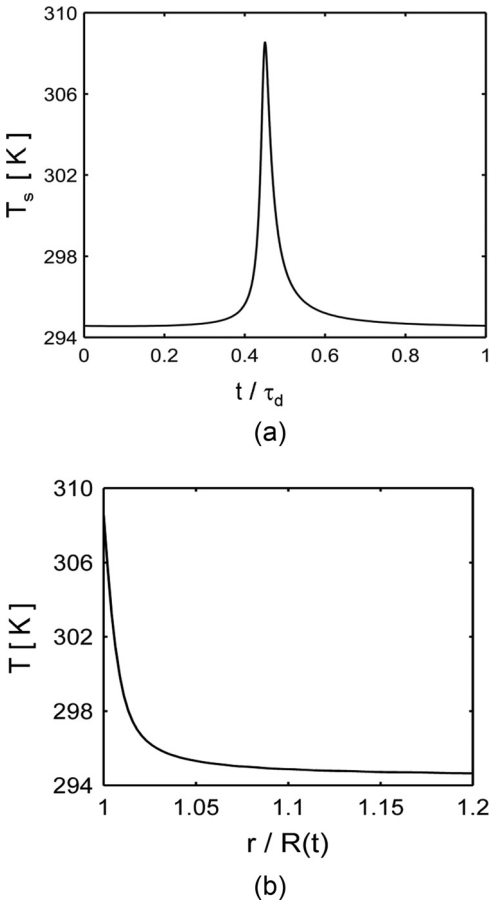

FIG. 2. (a) Liquid temperature at the bubble surface during the steady oscillations of an air bubble in water with an equilibrium radius of 130 μm driven at 20 kHz by a sound field with a pressure amplitude of 70 kPa; τ_d is the period of the sound field. (b) Liquid temperature distribution at the instant $t/\tau_d = 0.45$ at which the bubble wall of the previous figure reaches its maximum temperature.

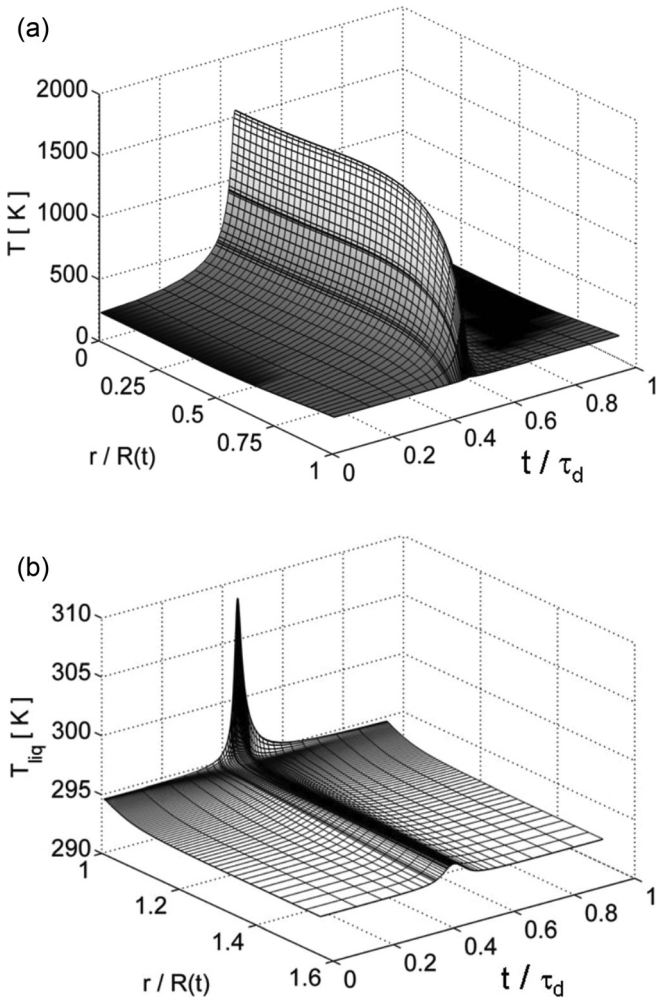

FIG. 3. Temporal and spatial evolution of temperature inside (a) and outside (b) a steadily oscillating 130 μm air bubble in water driven at 20 kHz by a sound field with a pressure amplitude of 70 kPa.

We now consider the effect of variations of the liquid temperature on the gas temperature and the radial dynamics of the bubble. The temperature T_s of the liquid at the bubble surface was estimated in 12 as

$$\frac{T_s - T_\infty}{T_{\text{center}} - T_s} = \sqrt{\frac{\lambda c_p \rho}{\lambda_L c_{p,L} \rho_L}} \tag{24}$$

with T_{center} the gas temperature at the bubble center, c_p the gas specific heat at constant pressure, and ρ a measure of the gas density. On this basis the expected liquid temperature

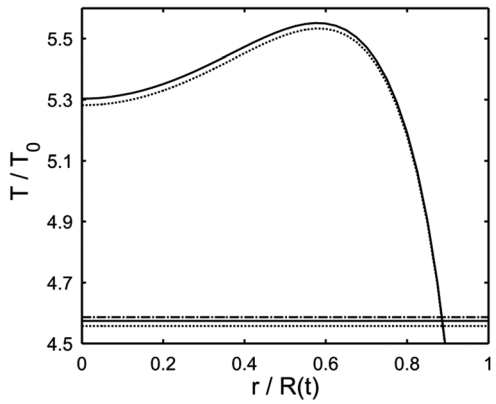

FIG. 4. Gas temperature distribution with a fixed (solid line) and a variable (dotted line) liquid temperature according to the detailed model. The dash-dot line shows the (average) temperature according to the simplified model and the horizontal solid and dotted lines are the average values of the detailed model. The temperatures are shown at the instants at which the peak value is reached in each case.

increase can be estimated to be small, but it is useful to go beyond estimates and determine quantitatively the actual importance of this effect.

Figure 2(a) shows the liquid temperature at the bubble surface as a function of time for the 130 μm-radius bubble driven at 20 kHz with a pressure amplitude of 70 kPa. The temperature distribution in the liquid in correspondence of the peak surface temperature is shown in Fig. 2(b). A space and time view of the temperature distribution in the gas and in the liquid in the course of a complete oscillation is provided in Fig. 3. It is seen that, even with oscillations of such relatively large amplitude, the maximum liquid temperature at the bubble surface increases by less than 15 K while the temperature at the core of the bubble becomes close to 1500 K. The shift in the absolute value of t/τ_d respect to Fig. 1 has no particular meaning, as it depends on where the origin of the acoustic cycle is taken.

The effect of the liquid temperature on the gas temperature is demonstrated in Fig. 4 which compares the gas temperature distributions taken at the instant at which the peak values are predicted allowing or not allowing for variations of the liquid temperature. The detailed model provides the entire gas temperature distribution (solid line), which is seen to be very little affected by the neglect of the liquid temperature rise (dotted line). The simplified model only gives the average temperature without liquid temperature variations (dash-dot line), which is seen to be very close to the average temperatures calculated with the detailed model.

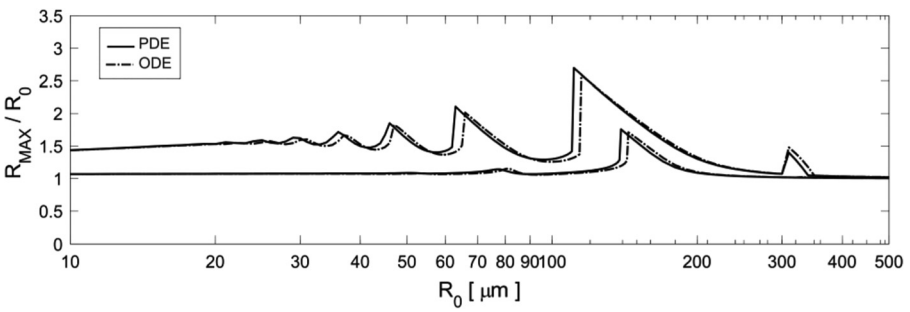

FIG. 5. Normalized maximum radius during the steady oscillations of an air bubble in water driven at 20 kHz as a function of the equilibrium radius R_0. The detailed and simplified model results are shown by the solid and dashed lines, respectively. In ascending order, the driving pressure amplitudes are 20 and 70 kPa.

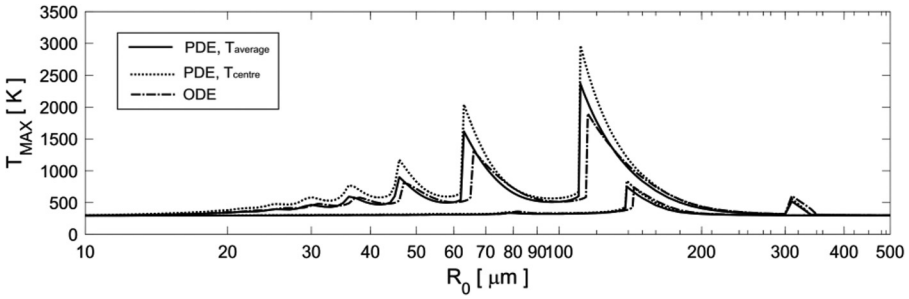

FIG. 6. Gas temperature at the center of the bubble (dotted line), and mean temperatures according to the detailed (solid line) and simplified (dash-dot line) models during the steady oscillations of an air bubble in water driven at 20 kHz as a function of the equilibrium bubble radius R_0. In ascending order, the driving pressure amplitudes are 20 and 70 kPa.

We conclude from these and other similar results not shown that temperature variations of the liquid have a negligible effect on the bubble gas temperature. This result is in line with the estimate (24) and the earlier results of Ref. 12. On this basis, in order to save computational time, in all the simulations described in the remainder of this paper we have kept the interface liquid temperature at the undisturbed value T_∞. Correspondingly, we have replaced Eq. (21) by the simpler condition

$$\sum_{k=0}^{N} \dot{a}_k = 0. \tag{25}$$

An overall impression of how the two models compare can be obtained from Fig. 5, where the normalized maximum radius during steady oscillations is shown as a function of the equilibrium radius R_0 for driving pressure amplitudes of 20 and 70 kPa; the sound frequency is 20 kHz as before. As already noted, the spherical shape is expected to be unstable at 70 kPa, but we consider this value of the pressure amplitude to bring into clearer evidence the differences between the two models.

As could be expected, the main differences are localized around the linear and nonlinear resonance peaks and are seen to grow with the driving amplitude. In general it is observed that, as R_0 increases, the transition to a large-amplitude regime (signaled by the vertical or nearly vertical line; see, e.g., Ref. 30 for an explanation of the nature of this transition) occurs slightly earlier in the detailed model than in the simplified one. As a consequence, the maximum amplitude reached by the detailed model is slightly higher but the difference remains small for the pressure amplitudes studied.

For sonochemical applications, a key aspect of the phenomenon of bubble oscillations is the gas temperature. Figure 6 shows the maximum value of this quantity as a function of R_0 for the same conditions as in Fig. 1. The center temperature for the detailed model is shown by the dotted line while the average temperature of the simplified model is indicated by the dash-dot line. The solid line is the volume-averaged temperature predicted by the detailed model and calculated from

$$\langle T \rangle = \frac{3}{R^3(t)} \int_0^R T(r,t) r^2 dr. \tag{26}$$

In correspondence with the larger maximum radius, the temperatures predicted by the detailed model are larger than that predicted by the simplified one, with a difference of a few hundred degrees attained in correspondence of slightly different radii near the main resonance at the largest driving amplitude. Just as in the case of the radius shown in Fig. 1, however, at the same value of the equilibrium radius the differences are not very large.

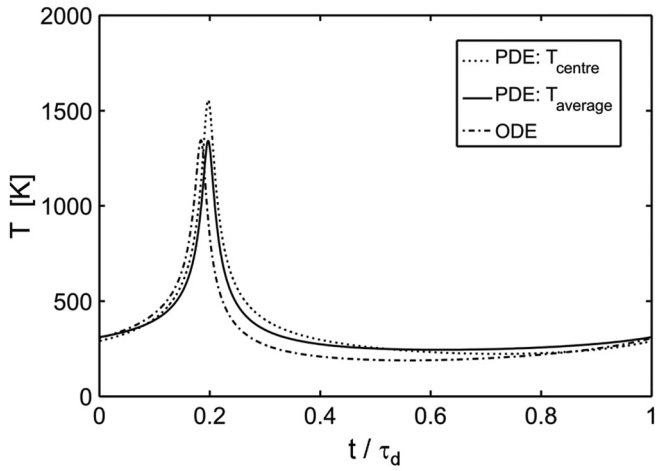

FIG. 7. Comparison between the temporal evolutions of the average temperature according to the simplified model (dash-dot line) and the center (dotted line) and average (solid line) temperatures of the detailed model during steady oscillations for the same conditions as in Fig. 1.

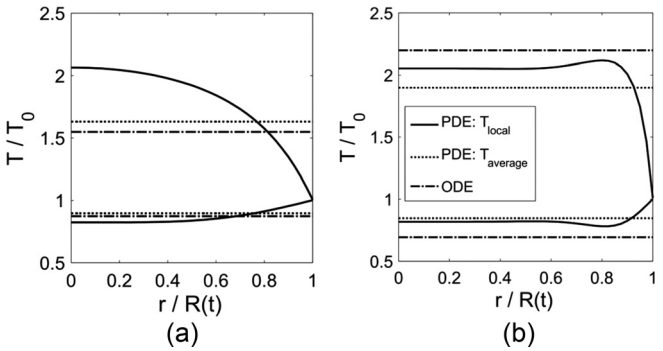

FIG. 8. Normalized temperature distribution inside air bubbles in water with equilibrium radii of 30 (a) and 305 (b) μm driven at 20 kHz by a sound pressure amplitude of 70 kPa. In each figure the upper and lower groups of three lines refer to the instants at which the peak and minimum average temperatures are attained. The solid lines are the results of the detailed model, the horizontal dash-dot line the average temperature from the simplified model and the dotted horizontal lines the average temperature of the detailed model calculated from Eq. (26).

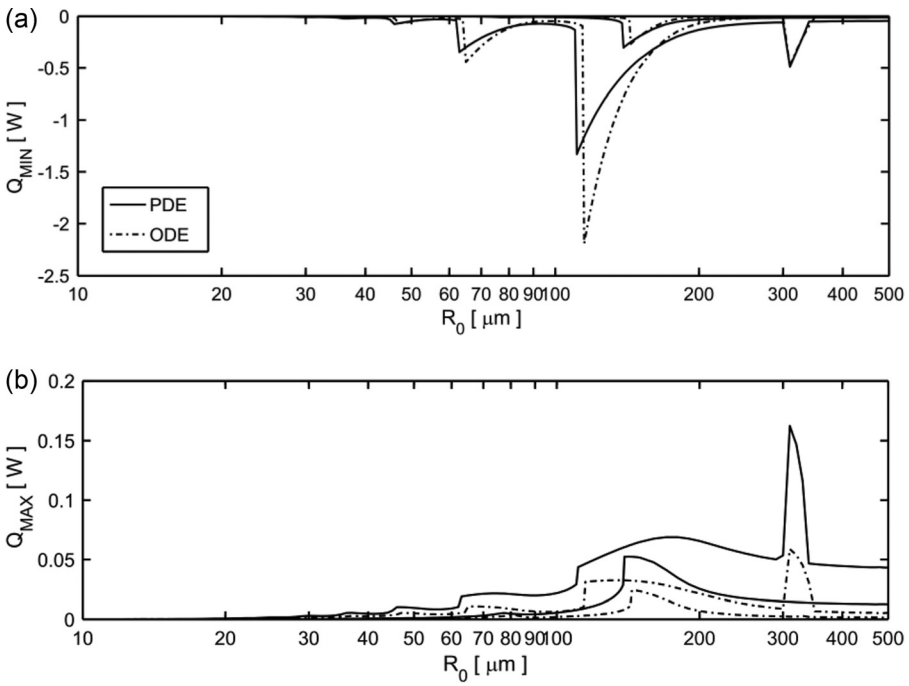

FIG. 9. Peak values of the heat lost (upper figure) and gained by a steadily oscillating air bubble in water driven at 20 kHz as a function of the equilibrium bubble radius R_0 according to the detailed (solid line) and simplified (dash-dot line) models. The sound pressure amplitudes are 20 and 70 kPa.

A more detailed view of the differences between the gas temperatures predicted by two models is shown in Fig. 7 for a 130 μm-radius bubble driven at 70 kPa and 20 kHz. The average temperatures of the detailed (solid line) and simplified (dash-dot line) models are nearly identical, while the center temperature of the detailed model peaks at a slightly higher value for a very short amount of time.

Figure 8 shows the normalized maximum and minimum temperature distributions inside bubbles with equilibrium radii of 30 and 305 μm driven at 70 kPa and 20 kHz. The solid and dotted lines are the local and average temperatures of the detailed model while the dash-dot lines are the average temperatures of the simplified model. The upper three lines refer to the instants at which the maximum average temperatures are reached in each model, and the lower three lines to the instants at which the minimum average temperatures are attained. The gas temperature distribution inside the largest bubble is approximately uniform except for a boundary layer near the wall. The temperature in the smallest bubble, on the other hand, exhibits a significant variation throughout the bubble volume. In this case the mean temperatures are very close, but the detailed distribution shows that this result comes about because the temperature in the inner region of the detailed model is offset by the relatively cool gas near the bubble wall. A good fraction of the gas is at a temperature about 20%–30% higher than the mean value. Given the at least approximate Arrhenius-law dependence of reaction rates, this difference in principle could have some observable effects in the sonochemical yield.

Related to the temperature distribution is the heat exchanged with the liquid which is given by Eq. (10) in the simplified model and by

$$Q = 4\pi R^2 \left[\lambda \frac{\partial T}{\partial r}\right]_{r=R(t)} \tag{27}$$

in the detailed model. The peak values of this quantity which, as defined, is positive when the transfer is directed from the liquid to the bubble, are shown in Fig. 9. The upper and lower diagrams show the heat lost and gained by the bubble, respectively. A major qualitative difference between the two diagrams is the respective orders of magnitude. The heat lost by the bubble is more than one order of magnitude larger than that gained. This feature is at the root of the dominance of thermal energy losses over other dissipative mechanisms affecting the oscillations of bubbles below and around the resonance frequency (provided the radius is not too small as to make viscous losses significant). The heat losses predicted by the detailed model (solid line, upper diagram) are close to those of the simplified model except in a narrow radius range near the fundamental resonance for the highest driving pressure, where they are seen to be around 40% smaller. This is a large difference, but it occurs only during the brief instants in which the bubble is close to its

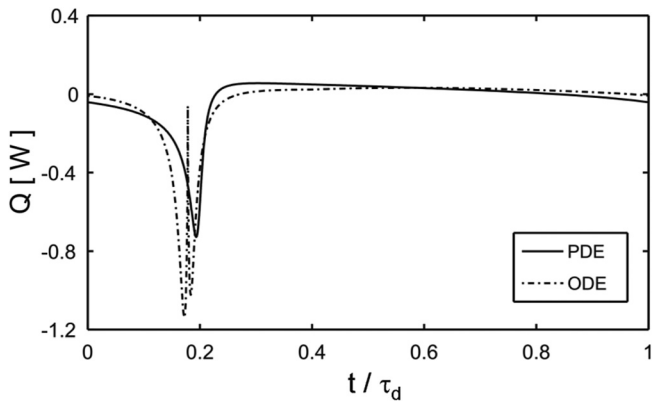

FIG. 10. Heat flow rate into the bubble as a function of time during the steady oscillations of a 130 μm-radius air bubble in water with driven at 70 kPa and 20 kHz as predicted by the detailed (solid line) and simplified models.

minimum radius, as shown in Fig. 10. The differences among the incoming heat flow rates are much larger, particularly from the second harmonic region on up, but the absolute values are small.

The distribution in time of the heat flow rate for the steady oscillations of a 130 μm-radius bubble driven at 70 kPa and 20 kHz is shown in Fig. 10. The solid line is the detailed model prediction and the dashed line that of the approximate model. The spike exhibited by the latter model near the point of maximum radius is an effect of the cutoff (12) applied when the boundary layer thickness becomes too large near the points of low radial velocity. This effect is highly localized in time and it is unlikely to have major consequences. In spite of the differences between the peak values shown in Fig. 9, one notices a substantial consistency between the two results over the complete course of an oscillation.

V. SUMMARY AND CONCLUSIONS

In this paper we have compared two models of the forced oscillations of gas bubbles in liquids, devoting particular attention to the gas temperature in view of its importance for sonochemistry. The two models differ in their ability to capture details of the process. One accounts for the temperature distribution in the bubble and in the surrounding liquid, while the other one treats the bubble as a spatially homogeneous system. We have found that when the oscillation amplitude is moderate, namely, at pressure amplitudes up to 70 kPa or, for larger pressures, away from linear and nonlinear resonances, the two models are in very good agreement. Thus, in this parameter range, the simpler model can be used with confidence with the advantage of simpler programming and shorter execution times. For strong driving or near resonances we have found some differences, but it is then doubtful that bubbles would retain their integrity in view of their susceptibility to shape instabilities and breakup.

We have focused on the single driving frequency of 20 kHz which is common in applications. At higher frequencies the picture would remain very similar provided radii are approximately shifted in inverse proportion to the frequency. Smaller bubbles, however, also tend to be more isothermal, with a consequent increase in energy loss. This feature is expected to reduce the difference between the two models at higher frequencies. The expectation is the opposite at lower frequencies, but larger bubbles are even more shape-unstable and, therefore, it is likely that neither model would be relevant except at rather low pressure amplitudes.

ACKNOWLEDGMENTS

This work is part of the research program of the Technology Foundation STW, which is financially supported by the Nederlandse Organisatie voor Wetenschappelijk Onderzoek (NWO).

[1]K. S. Suslick, "Sonochemistry," Science **247**, 1439–1445 (1990).
[2]K. S. Suslick, S. J. Doktycz, and E. B. Flint, "On the origin of sonoluminescence and sonochemistry," Ultrasonics **28**, 280–290 (1990).
[3]K. S. Suslick and G. J. Price, "Applications of ultrasound to materials chemistry," Annu. Rev. Mater. Sci. **29**, 295–326 (1999).
[4]*Sonochemistry and Sonoluminescence*, edited by L. A. Crum, T. J. Mason, J. L. Reisse, and K. S. Suslick (Kluwer Academic Publishers, Dordrecht, 1999), pp. 191–298.
[5]T. J. Mason and J. P. Lorimer, *Applied Sonochemistry, the Uses of Power Ultrasound in Chemistry and Processing* (Wiley-VCH, New York, 2002), pp. 1–22, 75–124.
[6]K. S. Suslick and D. J. Flannigan, "Inside a collapsing bubble: Sonoluminescence and the conditions during cavitation," Annu. Rev. Phys. Chem. **59**, 659–683 (2008).
[7]D. F. Gaitan, L. A. Crum, C. C. Church, and R. A. Roy, "Sonoluminescence and bubble dynamics for a single, stable, cavitation bubble," J. Acoust. Soc. Am. **91**, 3166–3183 (1992).
[8]L. A. Crum, "Sonoluminescence," Phys. Today **47**, 22–29 (1994).
[9]B. P. Barber, R. A. Hiller, R. Löfstedt, S. J. Putterman, and K. R. Weninger, "Defining the unknowns of sonoluminescence," Phys. Rep. **281**, 65–143 (1997).
[10]T. J. Matula, "Inertial cavitation and single-bubble sonoluminescence," Philos. Trans. R. Soc. London, Ser. A **357**, 225–249 (1999).
[11]M. P. Brenner, S. Hilgenfeldt, and D. Lohse, "Single bubble sonoluminescence," Rev. Mod. Phys. **74**, 425–484 (2002).
[12]V. Kamath, A. Prosperetti, and F. N. Egolfopoulos, "A theoretical study of sonoluminescence," J. Acoust. Soc. Am. **94**, 248–260 (1993).
[13]D. Lohse, M. P. Brenner, T. F. Dupont, S. Hilgenfeldt, and B. Johnston, "Sonoluminescing air bubbles rectify argon," Phys. Rev. Lett. **78**, 1359–1362 (1997).
[14]K. Yasui, "Alternative model of single-bubble sonoluminescence," Phys. Rev. E **56**, 6750–6760 (1997).
[15]K. Yasui, "Chemical reactions in a sonoluminescing bubble," J. Phys. Soc. Jpn. **66**, 2911–2920 (1997).
[16]W. C. Moss, D. A. Young, J. A. Harte, J. L. Levatin, B. F. Rozsnyai, G. B. Zimmerman, and I. H. Zimmerman, "Computed optical emissions from a sonoluminescing bubble," Phys. Rev. E **59**, 2986–2992 (1999).
[17]B. D. Storey and A. J. Szeri, "Water vapour, sonoluminescence and sonochemistry," Proc. R. Soc. London, Ser. A **456**, 1685–1709 (2000).
[18]B. D. Storey and A. J. Szeri, "A reduced model of cavitation physics for use in sonochemistry," Proc. R. Soc. London, Ser. A **457**, 1685–1700 (2001).
[19]R. Toegel, S. Hilgenfeldt, and D. Lohse, "Suppressing dissociation in sonoluminescing bubbles: The effect of excluded volume," Phys. Rev. Lett. **88**, 034301 (2002).
[20]R. Toegel and D. Lohse, "Phase diagrams for sonoluminescing bubbles: A comparison between experiment and theory," J. Chem. Phys. **118**, 1863 (2003).
[21]V. Kamath and A. Prosperetti, "Numerical integration methods in gas-bubble dynamics," J. Acoust. Soc. Am. **85**, 1538–1548 (1989).
[22]V. Q. Vuong and A. J. Szeri, "Sonoluminescence and diffusive transport," Phys. Fluids **8**, 2354–2364 (1996).
[23]H. Y. Cheng, M.-C. Chu, P. T. Leung, and L. Yuan, "How important are shock waves to single-bubble sonoluminescence?," Phys. Rev. E **58**, 2705–2708 (1998).
[24]H. Lin and A. J. Szeri, "Shock formation in the presence of entropy gradients," J. Fluid Mech. **431**, 161–188 (2001).
[25]R. Toegel, B. Gompf, R. Pecha, and D. Lohse, "Does water vapor prevent upscaling sonoluminescence?," Phys. Rev. Lett. **85**, 3165–3168 (2000).
[26]K. Yasui, T. Tuziuti, Y. Iida, and H. Mitome, "Theoretical study of the ambient-pressure dependence of sonochemical reactions," J. Chem. Phys. **119**, 346–356 (2003).
[27]M. S. Plesset and A. Prosperetti, "Bubble dynamics and cavitation," Annu. Rev. Fluid Mech. **9**, 145–185 (1977).
[28]T. G. Leighton, *The Acoustic Bubble* (Academic Press, London, 1994), pp. 84–86.
[29]C. E. Brennen, *Cavitation and Bubble Dynamics* (Oxford University Press, Oxford, 1995), pp. 47–67.
[30]A. Prosperetti, "Nonlinear oscillations of gas bubbles in liquids: steady-state solutions," J. Acoust. Soc. Am. **56**, 878–885 (1974).
[31]A. Prosperetti, "Thermal effects and damping mechanisms in the forced radial oscillations of gas bubbles in liquid," J. Acoust. Soc. Am **61**, 17–27 (1977).
[32]A. Prosperetti, L. A. Crum, and K. W. Commander, "Nonlinear bubble dynamics," J. Acoust. Soc. Am. **83**, 502–514 (1988).
[33]A. Prosperetti and Y. Hao, "Modelling of spherical gas bubble oscillations and sonoluminescence," Philos. Trans. R. Soc. London, Ser. A **357**, 203–223 (1999).
[34]D. Lohse and S. Hilgenfeldt, "Inert gas accumulation in sonoluminescing bubbles," J. Chem. Phys. **107**, 6986–6997 (1997).

[35]S. Hilgenfeldt, S. Grossmann, and D. Lohse, "A simple explanation of light emission in sonoluminescence," Nature **398**, 402–405 (1999).
[36]M. Plesset, "On the stability of fluid flows with spherical symmetry," J. Appl. Phys. **25**, 96 (1954).
[37]A. Prosperetti, "Viscous effects on perturbed spherical flows," Quart. Appl. Math. **34**, 339–350 (1977).
[38]M. P. Brenner, D. Lohse, and T. F. Dupont, "Bubble shape oscillations and the onset of sonoluminescence," Phys. Rev. Lett. **75**, 954–957 (1995).
[39]S. Hilgenfeldt, D. Lohse, and M. P. Brenner, "Phase diagrams for sonoluminescing bubbles," Phys. Fluids **8**, 2808–2826 (1996).
[40]R. G. Holt and D. F. Gaitan, "Observation of stability boundaries in the parameter space of single bubble sonoluminescence," Phys. Rev. Lett. **77**, 3791–3794 (1996).
[41]M. P. Brenner, T. F. Dupont, S. Hilgenfeldt, and D. Lohse, "Brenner *et al.* reply," Phys. Rev. Lett. **80**, 3668–3669 (1998).
[42]E. H. Trinh, D. B. Thiessen, and R. G. Holt, "Driven and freely decaying nonlinear shape oscillations of drops and bubbles immersed in a liquid: Experimental results," J. Fluid Mech. **364**, 253–272 (1998).
[43]D. F. Gaitan and R. G. Holt, "Experimental observations of bubble response and light intensity near the threshold for single bubble sonoluminescence in an air-water system," Phys. Rev. E **59**, 5495–5502 (1999).
[44]Y. Hao and A. Prosperetti, "The effect of viscosity on the spherical stability of oscillating gas bubbles," Phys. Fluids **11**, 1309–1317 (1999).
[45]M. Versluis, D. E. Goerts, P. Palanchon, I. L. Heitman, S. M. van der Meer, B. Dollet, N. de Jong, and D. Lohse, "Microbubble shape oscillations excited through ultrasonic parametric driving," Phys. Rev. E **82**, 026321 (2010).
[46]A. Prosperetti, "The thermal behavior of oscillating gas bubbles," J. Fluid Mech. **222**, 587 (1991).
[47]R. Toegel, S. Hilgenfeldt, and D. Lohse, "The effect of surfactants on single bubble sonoluminescence," Phys. Rev. Lett. **84**, 2509–2512 (2000).
[48]Visual Numerics, "IMSL Numerical Libraries," http://www.vni.com/products/imsl/ (Last viewed 3/09/2011).
[49]L. H. Thompson and L. K. Doraiswamy, "Sonochemistry: Science and engineering," Ind. Eng. Chem. Res. **38**, 1215–1249 (1999).